Supplementary Materials for the paper

Universal Time Variations in Space Weather

M. Lockwood, M.J. Owens, C. Haines, L.A. Barnard, C.J. Scott, A. Chambodut, K.A. McWilliams and A.W.P. Thomson

Submitted to Geophysical Research Letters

Abstract. We here present details of some of the factors used in the main publication and give polynomial fits that are used in the production of the modelled F-UT patterns of geomagnetic activity indices presented.

Contents:

(i). Estimation of Power input into the magnetosphere

We use 1-minute data on the solar wind and interplanetary magnetic field, available from 1980 onwards as the Omni2 dataset from the Space Physics Data Facility (SPDF) at NASA's Goddard Space Flight Center: https://omniweb.gsfc.nasa.gov/ow_min.html, to estimate the power input into the magnetosphere using the equation (see Lockwood, 2019 and references therein:

$$P_\alpha = \left(\pi k_2 k_1^2 M_E^{2/3} \mu_0^{-1/3}\right) m_{sw}^{(2/3-\alpha)} N_{sw}^{(2/3-\alpha)} V_{sw}^{(7/3-2\alpha)} B^{2\alpha}\, sin^4(\theta/2) \quad (1)$$

where k_1 and k_2 are constants; M_E is the magnetic moment of the Earth which can be computed for a given time using the IGRF-15 Model (Thébault et al., 2015), μ_0 is the permeability of free space (the magnetic constant); m_{sw} is the mean ion mass, N_{sw} the number density and V_{sw} is the speed of the solar wind at Earth; B is the near-Earth Interplanetary Magnetic Field (IMF) and θ is the clock angle the IMF makes with the Z-

direction of the Geocentric Solar Magnetospheric frame of reference; α is called the coupling exponent and is the one free fit parameter. We use the optimum value of $\alpha = 0.44$ that yields the maximum correlations with the am index: Lockwood (2019) shows that these are 0.79 for the 3-hourly basic resolution of the am data, 0.91 for daily means, 0.93 for Carrington rotation means and 0.98 for annual means (all of which are highly statistically significant giving p values for the null hypothesis of less than 0.0001). The mean ion mass m_{SW} generally only available at hourly or 15 second resolution and are linearly interpolated to the 1-minute resolution, a procedure that readily meets the 5% error limit adopted in tests using the available 15-second resolution data. The 1-minute P_α data are then averaged into hourly intervals. Data gaps are handled using the criteria for the required number of samples for each parameter that ensures that the error in hourly P_α value is below 5%. These criteria were established by *Lockwood et al* (2018) by introducing synthetic data gaps into continuous data. Hourly intervals not meeting these criteria in all parameters were treated as data gaps in the P_α data series.

(ii). Time-of-day/time-of-year pattern plots

The patterns with fraction of a calendar year (F) and Universal Time (UT) are generated by averaging the hourly data for each UT in 36 equal width bins of F (each just over 10 days in width). This yields 864 bins and we applying a 2-dimensonal 1-3-1 triangular weighting smooth in both the F and UT dimensions. For the observations the am, an, and as data are linearly interpolated to hourly values from the 3-hourly indices using linear interpolation.

(iii). Calculation of the hemispheric conductivity factors, $P_{\Sigma N}$ and $P_{\Sigma S}$

In theory, conductivities could be evaluated for every location in the polar regions using empirical relationships for a given solar zenith angle, χ. However this leaves the problem as to which locations most influence the an and as hemispheric sub-indices (and hence $am = (an + as)/2$): for example, what is the dependence on conductivity in the auroral oval compared to that over the observing magnetometer? Hence we take an empirical approach using means over several days of the deviations of an and as from am that average out the UT variations and studying the dependence of $\Delta an = (an - am)$ and $\Delta as = (as - am)$ with F and compare with the corresponding variations of the mean dipole tilt angle, ψ. Figure S1 shows the results.

The best 4th-order polynomial fit for the northern hemisphere index an is

$$\Delta an/an \; = \; 1.064 \times 10^{-8}\, \psi(F)^4 + 2.840 \times 10^{-6}\, \psi(F)^3$$

$$+ \, 1.910 \times 10^{-5}\, \psi(F)^2 + 1.695 \times 10^{-3}\, \psi(F) - 0.884 \times 10^{-2}$$

The factor $P_{\Sigma N}$ converts an ideal value of an (an_{cc}) into what we actually observe (an), such that

$$an = \; P_{\Sigma N} \times an_{cc}$$

If, for a first order correction we take am to be a good estimate of an_{cc} on the approximately 10-day timescales considered in Figure S1, then $an_{cc} = an - \Delta an = \; an/P_{\Sigma N}$

hence the northern hemisphere conductivity factor is $P_{\Sigma N} = (1 - \Delta an/an)^{-1}$ and likewise that for the southern hemisphere, $P_{\Sigma S} = (1 - \Delta as/as)^{-1}$.

The best 4th-order polynomial fit for the southern hemisphere index as is

$$\Delta as/as = -0.948\times10^{-8}\,\psi(F)^4 - 3.137\times10^{-6}\,\psi(F)^3$$

$$-2.238\times10^{-5}\,\psi(F)^2 - 1.138\times10^{-3}\,\psi(F) - 0.988\times10^{-2}$$

The corrected indices, $an_{cc} = an/P_{\Sigma N}$, $as_{cc} = as/P_{\Sigma S}$ and $am_{cc} = (an_{cc} + as_{cc})/2$ are shown in Figure S1b. Note that the corrections make an_{cc} and as_{cc} very similar indeed. Note also that the resulting am_{cc} is not exactly the same as am: the semi-annual variation in am_{cc} is slightly larger in amplitude and there is different structure around the peaks (which is also seen in both an_{cc} and as_{cc}). This indicates that the conductivity effects in the two hemisphere do not exactly cancel in am. The residuals for the polynomial fits give a percentage root mean square (r.m.s.) error in $P_{\Sigma N}$ and $P_{\Sigma S}$ of just 0.21%.

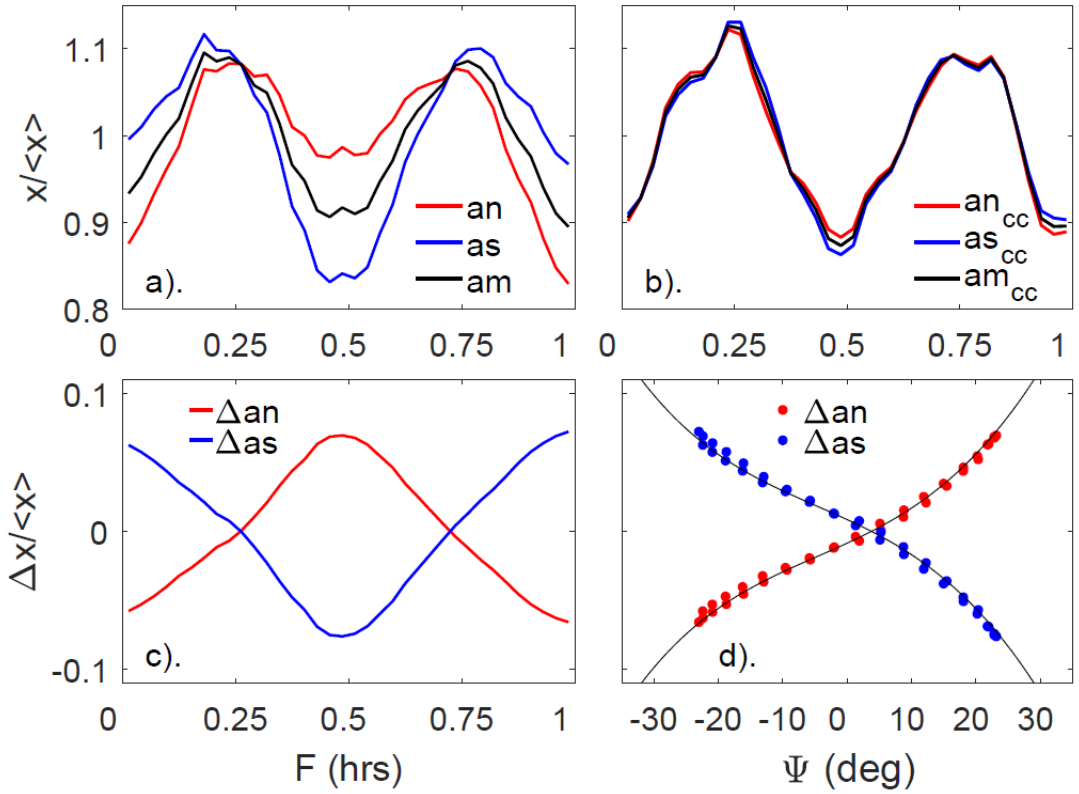

Figure S1. (a) The observed variations of the geomagnetic indices with fraction of year, shown as a fraction of their overall mean: (red) $an(F)/< an >_{all}$; (blue) $as(F)/< as >_{all}$; and (black) $am(F)/< am >_{all}$. (b) The variations after correction for conductivity effects (using the factors derived): (red) $an_{cc}(F)/< an_{cc} >_{all}$; (blue) $as_{cc}(F)/< as_{cc} >_{all}$; and (black) $am_{cc}(F)/< am_{cc} >_{all}$. The deviations of an and as from am, (red) $\Delta an = an - am$, (blue) $\Delta as = as - am$, which for the 36 bins in F (≈10-day timescale) are taken to be due to conductivity effects alone. (d) The variations of (red points) Δan and (blue points) Δas as a function of the mean dipole tilt angle, ψ for the same F-UT. The black lines are 4th-order polynomial fits to the points.

(iv). Eccentric dipole axial pole locations and velocities in the GSEQ frame

The eccentric dipole axis $\vec{M}$ (a dipole axis not constrained to pass through the Earth's centre) was taken from the work of *Koochak and Fraser-Smith* (2017) using the coefficients for the two axial pole locations that were linearly interpolated from their tabulated values to the middle date of the am data interval under consideration. The location and motion of the eccentric axial poles in geographic coordinates into the GSEQ frame using the CXFORM Coordinate transformation package originally written by Ed Santiago of Los Alamos National Laboratory and Ryan Boller of NASA's Goddard Space Flight Centre and re-programmed for Matlab by Patrik Forssén (SatStar Ltd & Karlstad University) in 2017, available from https://spdf.sci.gsfc.nasa.gov/pub/software/old/selected_software_from_nssdc/coordinate_transform/#Mi. This software package is based on the equations by Mike Hapgood of RAL Space, Rutherford Appleton Laboratory (*Hapgood*, 1992).

GSEQ locations of the poles at an altitude of 800 km (in the topside ionosphere) were computed at the 36 values of F and for three times around the 24 hourly UT values, these times being shifted by −1min, 0 and +1min from each UT value and the velocities $[V_X]_{NP}$ and $[V_X]_{SP}$ computed from the difference in the X coordinates for the −1min, and +1min cases.

(v). The pole motion factors P_{PM}

The sunward motion (in the $+X$ direction) in the GSEQ frame of the northern axial pole at speed $[V_X]_{NP}$ generates a modulation to the northern ionospheric cap transpolar voltage in that frame of

$$\Delta\Phi_{cfN} = d \times < B_{iYZ} > \times [V_X]_{NP}$$

where d is the polar cap diameter and $< B_{iYZ} >$ is the ionospheric magnetic field normal to the X direction. The average effect for the two polar caps is then

$$\Delta\Phi_{cf} = \frac{\Delta\Phi_{cfN} + \Delta\Phi_{cfS}}{2} = d \times < B_{iYZ} > \times \frac{([V_X]_{NP} + [V_X]_{SP})}{2}$$

and $P_{PM}(UT) = \Delta\Phi_{cf} / \Phi_{cf}$

where we compute Φ_{cf} for a given am from the regression equation given by equation (A4) in Appendix A of *Lockwood et al*. (2020b).

$$\Phi_{cf} = (6.68 \times 10^{-5}) am^3 - (1.66 \times 10^{-2}) am^2 + 1.89 am + 6.17$$

(vi). Russell-McPherron factor P_{RM}

The CXFORM Coordinate transformation package was also used to compute the GSEQ to GSM transformation of unit IMF vectors in the $+Y$ and $-Y$ directions of GSEQ and give the IMF clock angle θ and hence the Russell-McPherron predictions of the $sin^4(\theta/2)$ IMF orientation factor in P_α and hence the factor $P_{RM}(F, UT)$. Note that in the original paper, Russell and McPherron (1973) used a half-wave rectified southward component IMF orientation factor (B_S/B) whereas we employ $sin^4(\theta/2)$: these two have been compared and discussed by Lockwood et al. (2020b).

(vii). Dipole tilt angle, ψ

The dipole tilt angle was computed as a function of F and UT, being the angle between $\vec{M}$ and the $\vec{S}$, the geocentric position vector of the subsolar point, computed using the SUBSOL routine of the LOWTRAN7 Sun and Moon Models Matlab package generated by Noah of the US Air Force Geophysics Laboratory in 2019 and available from https://www.mathworks.com/matlabcentral/fileexchange/71203-lowtran7-sun-and-moon-models?s_tid=FX_rc1_behav .

(viii). The tail squeezing factor $P_\psi(\psi)$

This factor was modelled by *Lockwood et al.* (2020b;c) using the asymmetric magnetopause location model of *Lin et al.* (2017) by assuming that the tail is in equilibrium with a solar wind of dynamic pressure p_{sw}. Figure S2. shows the variations with tilt angle derived.

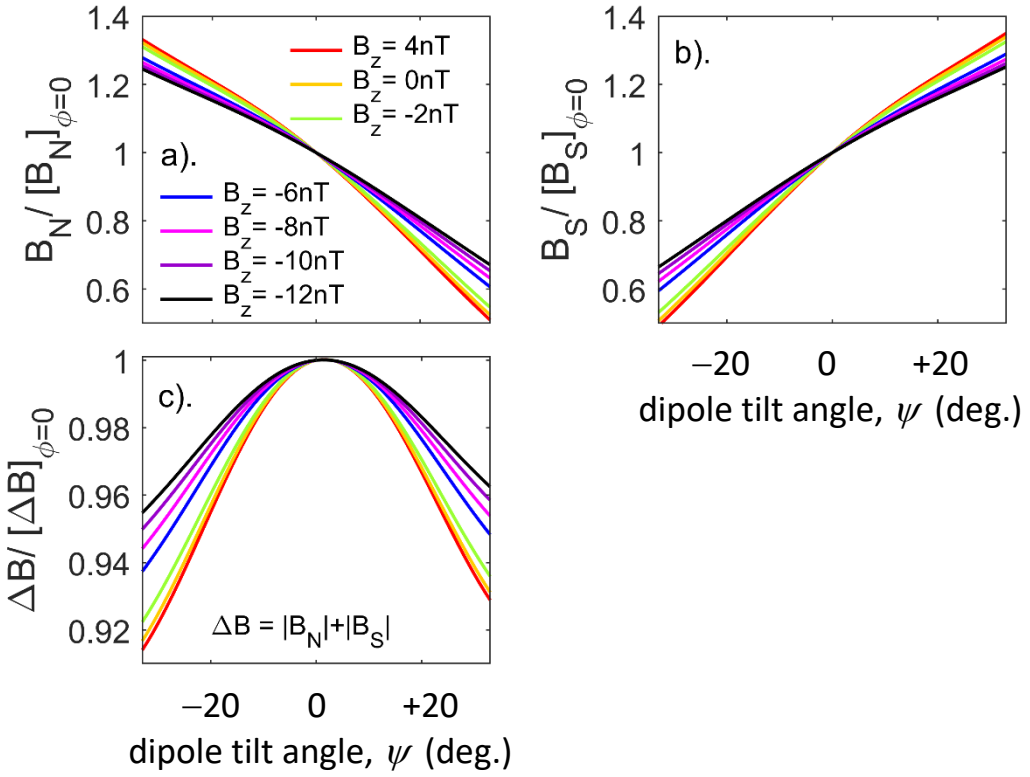

Figure S2. (Top panels) The modelled maximum lobe field along the bisector of the tail hinge angle, evaluated from the magnetopause location and magnetosheath pressure for the Newtonian approximation by assuming the tail is in equilibrium, and shown as a function of the dipole tilt angle ψ for various values of the IMF B_z and the mode values of the distributions of solar wind static and dynamic pressures for 1980-2018 of p_{st} = 0.015 nPa and p_{SW} = 1.50 nPa. (a) shows the field in the northern lobe, B_N, (b) shows that in the southern lobe, B_S, both as a ratio of their values for ψ =0. The fall in B_N with increasing ψ is mirrored by a rise in B_S, but not quite exactly: this can be seen in part (c) that shows the magnetic shear across the hinge in the current sheet $\Delta B = |B_N| + |B_S|$ which is proportional to the current per unit length in the cross-tail current sheet (again plotted values are normalized to the value for ψ =0, $[\Delta B]_{\phi=0}$. In all panels the various colors are for different IMF $[B_Z]_{GSM}$ inputs to the magnetopause model that vary from +4nT (red) to −12nT (black). It can be see that ΔB is

largest for $\psi = 0$ but is also larger for large positive ψ than large negative ψ. This is a consequence of the hemispheric asymmetry in the magnetopause model.

A 4th order polynomial that fits (with scaling) all the variations of ΔB in Figure S2c that is accurate to within an r.m.s. error of 0.02% is

$$P_{\psi\Delta B}(\psi) = 3.645\times10^{-8}\psi^4 - 1.059\times10^{-7}\psi^3 - 1.115\times10^{-4}\psi^2 + 4.768\times10^{-4}\psi + 1$$

Lockwood et al. (2020b) show that the equinoctial pattern in the am index increases linearly in amplitude with solar wind dynamic pressure and fitting the above functional form $P_{\psi\Delta B}(\psi)$ to the pattern amplitude the find for am observations for the mode value of p_{SW} of 1.50 nPa yields

$$P_{\psi}(\psi) = 1 + 3.80\times\{P_{\psi\Delta B}(\psi) - 1\}$$